RSC Advances

PAPER

Cite this: *RSC Adv.*, 2016, **6**, 54001

Transport properties of Co-based Heusler compounds Co_2VAl and Co_2VGa: spin-polarized DFT+U

A. H. Reshak*[ab]

Transport properties of two Co-based Heusler compounds Co_2VAl and Co_2VGa were calculated. The calculated spin-polarized electronic band structures for majority and minority spin reveal that the minority spin exhibits an indirect band gap of about 0.3 eV for Co_2VAl and 0.2 eV for Co_2VGa. It is clear that the minority spin density of states at E_F, $N(E_F)$ vanishes for Co_2VAl and Co_2VGa which leads to unusual transport properties because only the majority density contributes to the states at E_F. The calculated valence band's electronic charge density distribution reveals that there exists a strong covalent bond between the atoms which is more favorable for the transport of carriers than an ionic one. The transport properties were calculated as a function of temperature at a fixed chemical potential and as a function of chemical potential at three constant temperatures. In Co_2VAl a large value (1100 $\mu V\ K^{-1}$) of Seebeck coefficient is obtained for spin-down electrons due to the existence of an almost flat conduction band along the L to Γ direction. Calculations show that Co_2VAl exhibits a higher Seebeck coefficient than that obtained from Co_2VGa and the increase in the Seebeck coefficient also leads to a maximum in the power factor. This makes the Co_2VAl and Co_2VGa compounds attractive candidates for materials used in spin voltage generators.

Received 20th April 2016
Accepted 18th May 2016

DOI: 10.1039/c6ra10226c

www.rsc.org/advances

1. Introduction

Recently, Heusler compounds had an astonishing comeback. Because of their high spin polarization and their high Curie temperatures they have received exceptional attention for possible applications in the field of spin-electronics, magneto-resistive devices (spintronics) and thermoelectric devices.[1–3] Recent review articles cover the basic physics of half-metallic ferromagnets (HMF)[1] and aspects of their applications.[2,3] The properties of Heusler compounds are strongly dependent on the atomic order. Band structure calculations show that already small amounts of disorder within the distribution of the atoms on the lattice sites cause distinct changes in their electronic structure, and thus also in their magnetic and transport properties.[4–6] Therefore, a careful analysis of their crystal structure is essential to understand the structure-to-property relation of Heusler compounds. The transition from the ordered to the most prominent disordered Heusler structures (X_2YZ) will be explained as follows;[7–11] if the Y and the Z atoms are evenly distributed, the 4a and 4b positions become equivalent. This leads to a CsCl-like structure, also known as B2-type disorder. The symmetry is reduced and the resulting space group is $Pm\bar{3}m$. The random distribution of X and Y or X and Z leads to BiF_3-type disorder (space group $Fm\bar{3}m$). Already small amounts of anti-site disorder cause changes in the electronic structure close to the Fermi energy, which lead to altered physical properties. The existence of martensitic transition in Heusler alloys makes them potential candidates for actuation devices and smart materials.[12–16]

The recent observation of the spin Seebeck effect allows a pure spin current to pass over a long distance[17] and is directly applicable to the production of spin voltage generators which are crucial for driving spintronics devices.[18–20] Recently, half-metallic compounds have attracted much interest because of their exceptional band structures at the Fermi level (E_F). From the electronic band structure point of view, half-metals have metallic character for one spin channel and semiconducting for the other.[21] There exists a high spin-polarization at the E_F and many Heusler alloys belong to this family.[21] Therefore, we think it would be worthwhile to investigate the electronic structure and hence the transport properties of two Co-based Heusler compounds (*i.e.* Co_2VAl and Co_2VGa). The calculations have been performed in order to understand the properties of the band gap in the minority spin channel and the peculiar transport properties of the Co_2VAl and Co_2VGa compounds.

2. Details of calculations

The Co-based Heusler compounds Co_2VAl and Co_2VGa crystallize in cubic symmetry with the $Fm\bar{3}m$ space group.[22,23] The experimental lattice constants are $a = 5.770$ Å (ref. 22 and 23)

[a]*New Technologies-Research Centre, University of West Bohemia, Univerzitni 8, 306 14 Pilsen, Czech Republic. E-mail: maalidph@yahoo.co.uk; Fax: +420 386 361255; Tel: +420 777729583*

[b]*Center of Excellence Geopolymer and Green Technology, School of Material Engineering, University Malaysia Perlis, 01007 Kangar, Perlis, Malaysia*

for Co_2VAl and $a = 5.786$ Å (ref. 22 and 23) for Co_2VGa. Using the generalized gradient approximation (PBE-GGA)[24] we have optimized the lattice constants. These are $a = 5.751$ Å for Co_2VAl and $a = 5.763$ Å for Co_2VGa, which show good agreement with the experimental data.[22,23] The full potential linear augmented plane wave plus the local orbitals (FPLAPW + lo) method as implemented in the WIEN2k code[25] within PBE-GGA was used to perform comprehensive calculations for the Co_2VAl and Co_2VGa compounds. It is well-known that for oxides and other highly correlated compounds, local density approximation (LDA) and the generalized gradient approximation (GGA) are known to fail to give the correct ground state. In these systems, the electrons are highly localized. The Coulomb repulsion between the electrons in open shells should be taken into account. As there is no exchange correlation function that can include this in an orbital independent way, a simpler approach is to add the Hubbard-like on-site repulsion to the Kohn–Sham Hamiltonian. This is known as an LDA+U or GGA+U calculation. There are different ways in which this can be implemented. In the present work, we used the method of Anisimov *et al.*[26] and Liechtenstein *et al.*[27] where the Coulomb (U) and exchange (J) parameters are used. From the obtained relaxed geometry the ground state properties were determined using FPLAPW + lo[25,28,29] within GGA+U (U-Hubbard Hamiltonian). We applied U on the 3d orbital of Co atoms and V atoms, and we have tested several U values until we reached the energy band gap values that agree well with the previous results.[30] The U values used here are 0.15 Ryd and 0.187 Ryd (ref. 30) for Co and V, respectively. Based on the calculated electronic band structures we have calculated the transport properties of Co_2VAl and Co_2VGa utilizing the semi-classical Boltzmann theory as incorporated within the BoltzTraP code.[31] Simulations of the transport properties are a transition from first- to second-principles methods. The first-principles method used here is the all-electron full potential linear augmented plane wave method whereas the second-principles method is the BoltzTraP code,[31] which solves the semi-classical Bloch–Boltzmann transport equations.[31] Transport properties were obtained from the ground state within the limits of the Boltzmann theory[32–34] and the constant relaxation time approximation as implemented in the BoltzTraP code.[31] In short, BoltzTraP performs a Fourier expansion of the quantum chemical band energies. This allows us to obtain the electronic group velocity v and inverse mass tensor, as the first and second derivatives of the bands with respect to k. Applying v to the semi-classical Boltzmann equations, the transport tensors can be evaluated.

The potential for the construction of the basis functions inside the sphere of the muffin-tin was spherically symmetric, whereas it was constant outside the sphere. Self-consistency is obtained using 800 $\vec{k}$ points in the irreducible Brillouin zone (IBZ). The self-consistent calculations are converged since the total energy of the system is stable within 0.00001 Ryd. The spin-polarized electronic band structure and the transport properties were performed within 20 000 $\vec{k}$ points in the IBZ as the accurate calculations of transport properties of metals require dense sampling of the Brillouin zone. It is well known that first-principles calculations are a powerful and useful tool to predict the crystal structure and its properties related to the electron configuration of a material before its synthesis.[35–37]

3. Results and discussion

3.1. Salient features of the spin-polarized electronic band structure

The calculated spin-polarized electronic band structures for the spin-up (↑) majority spin and spin-down (↓) minority spin are shown in Fig. 1b, d, g and i. It has been found that the minority spin exhibits an indirect band gap of about 0.3 eV for Co_2VAl and 0.2 eV for Co_2VGa, as the valence band maximum (VBM) is located at the Γ point of the BZ and the conduction band minimum (CBM) at the X point of the BZ. The obtained values using GGA+U are much better than the previous calculated energy band gap of 0.238 eV (0.189 eV) of Co_2VAl (Co_2VGa) using LDA+U.[38] Meanwhile, the majority spin exhibits a metallic structure with a density of states at E_F, $N(E_F)$ of about 15.30 (state per eV per unit cell) for Co_2VAl and 13.22 (state per eV per unit cell) for Co_2VGa. The calculated density of states at E_F enables us to calculate the bare electronic specific heat coefficient (γ) which is about 2.65 and 2.29 mJ per mol cell K^2 for Co_2VAl and Co_2VGa. It is clear that the minority spin density of states at E_F, $N(E_F)$ vanishes for Co_2VAl and Co_2VGa which should lead to unusual transport properties because only the majority density contributes to the states at E_F. Similar behavior was observed in the Co_2MnAl and Co_2MnSn compounds.[39] Therefore, the bands which cross E_F are responsible for the transport properties of the compound and those bands which are not crossing E_F will contribute negligibly to the transport properties.[21] The calculated Fermi surface of the majority spin for Co_2VAl and Co_2VGa are shown in Fig. 1a and f. We noticed that in the Fermi surface there are white regions which represent the hole concentration while the colored regions correspond to the presence of electrons.[40] The colors of the Fermi surface also give an idea about the speed of the electrons. The red color represents the highest speed, yellow, green and blue have intermediate speeds whereas the violet color shows the lowest speed. The colors of the Fermi surface confirm that replacing Al by Ga causes reduction/increase in the speed of the electrons at the Fermi surface. Usually the transport properties are related to the electrons in the system, and these electrons are defined through the Fermi surface, which determines the electrical conductivity.[40]

Our results reveal that the Co_2Val and Co_2VGa compounds exhibit half-metallic (HM) nature. The electronic band structure in the area around the CBM and the VBM show that both CBM and VBM have parabolic bands in the vicinity of the Fermi level (Fig. 1b, d, g and i). This implies that Co_2Val and Co_2VGa show highest k-dispersion bands around E_F and thus lowest effect masses and hence the highest mobility carriers.

To obtain further insight into the type of states associated with each orbital, the projected density of states (DOS) were calculated. The angular momentum character of various structures in the Co_2VAl and Co_2VGa compounds for the spin up (↑) and spin down (↓) states can be obtained by calculating the angular momentum projected density of states (PDOS), as shown in Fig. 2a–d. It is demonstrated that replacing Al by Ga

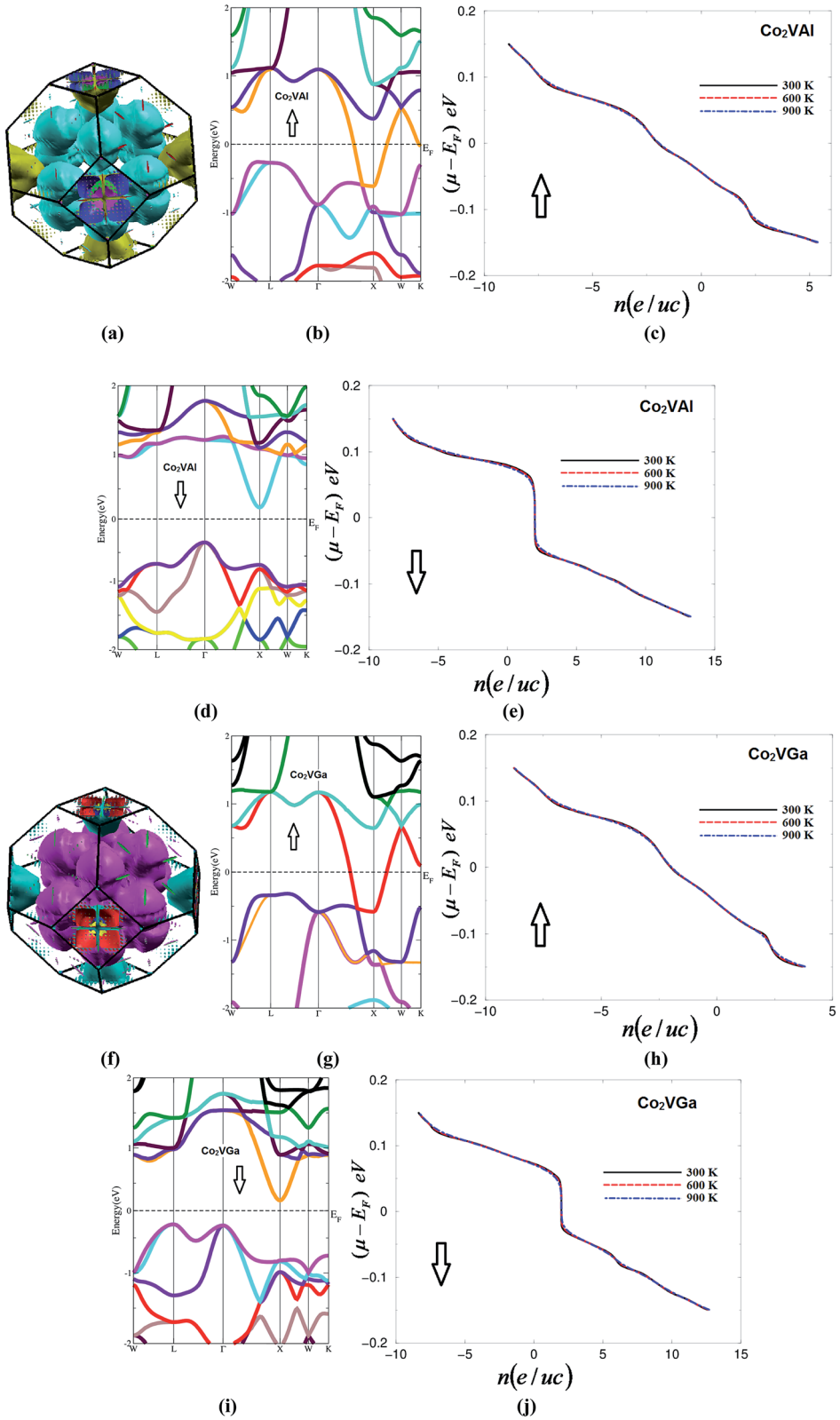

Fig. 1 (a) Calculated Fermi surface of the Co_2VAl compound. The white regions represent the hole concentration while the colored regions correspond to the presence of electrons. The red color represents the highest speed, yellow, green and blue have intermediate speeds whereas the violet color shows the lowest speed; (b) calculated spin-up electronic band structure of the Co_2VAl compound; (c) calculated carrier concentration as a function of chemical potential ($\mu - E_F = \pm 0.2$ eV) at three constant temperatures (300, 600 and 900 K) for the spin-up configuration of the Co_2VAl compound; (d) calculated spin-down electronic band structure of the Co_2VAl compound; (e) calculated carrier concentration as a function of chemical potential ($\mu - E_F = \pm 0.2$ eV) at three constant temperatures (300, 600 and 900 K) for the spin-down configuration of the Co_2VAl compound; (f) calculated Fermi surface of the Co_2VGa compound. The white regions represent the hole

introduces high peaks in the density of states below E_F and that the charge density near the DOS peaks is substantially attracted toward Ga atoms due to their high electro-negativity.[41] It is clear that the Co-s/p/d, V-s/p/d and Ga-s/p/d (Al-s/p) orbitals are distributed in the valence and conduction bands along the whole energy scale and this shows that there exists a strong hybridization between the states, for instance in the Co_2VAl compound the Al-p state is hybridized with the Co-s/p and V-s/p states, Al-s with V-s and Co-s, and Co-d with V-d. Meanwhile, for the Co_2VGa compound the Ga-p state hybridized with the Co-s/p and V-s states, Co-s/p with the Ga-s and V-p states, and Co-d with the V-d state. The hybridization degree favors enhancing the covalent bonding.[42] To support this statement we have calculated the valence band electronic charge density distribution of the Co_2VAl and Co_2VGa compounds.

3.2. Valence electronic charge density

To visualize the charge transfer and the chemical bonding character, the valence band electronic charge density distributions are calculated and analyzed in detail. Fig. 3a–i illustrates the calculated total valence charge density distribution in two crystallographic planes along the (1 0 0) and (1 0 1) directions for spin-up and spin-down cases. According to the Pauling scale, the electro-negativities of Co, V, Al and Ga atoms are 1.88, 1.63, 1.61 and 1.81, respectively. Thus the electro-negativity differences between the atoms are small, therefore the small electro-negativity differences indicate that there exist covalent bonds.[43,44] Covalent bonding is more favorable for the transport of carriers than ionic bonding.[45] Also, due to the electro-negativity differences between Co, V, Al and Ga atoms, some valence electrons are transferred towards Co and Ga atoms as it is clear that the Co and Ga atoms are surrounded by uniform blue spheres which indicate the maximum charge accumulation according to the thermoscale (Fig. 3i). We would like to highlight that the crystallographic plane along the (1 0 0) direction shows only Al(Ga) and V, whereas the crystallographic plane along the (1 0 1) direction shows all atoms. Therefore, the calculated valence band's electronic charge density distribution helps us to gain deep insight into the nature of the chemical bonding, anisotropy in bonding and to explore the transport of the carriers.

3.3. Transport properties

3.3.1. Charge carrier concentration and electrical conductivity. We have investigated the influence of temperature on the carrier concentration of the Heusler compounds Co_2VAl and Co_2VGa for the majority and minority spin at a certain value of the chemical potential ($\mu = E_F$). It has been found that the carrier concentration of the majority spin increases exponentially with increasing temperature as illustrated in Fig. 4a and b and the negative sign indicates that the materials exhibit n-type conduction, whereas for the minority spin the carrier concentration (Fig. 4c and d) shows a constant value until 400 K (450 K) for Co_2VAl (Co_2VGa), then increases dramatically with increasing temperature and the materials exhibit p-type conduction. The observed trends of the carrier concentration for the majority and minority spin confirm the half-metallic (HM) nature of Co_2VAl and Co_2VGa. To support this statement we have investigated the carrier concentration for ($\uparrow$) and ($\downarrow$) at three constant temperatures (300, 600 and 900 K) and $\mu - E_F = \pm 0.2$ eV in the vicinity of the Fermi level as shown in Fig. 1c, e, h and j. It has been noticed that the difference between chemical potential and Fermi energy ($\mu - E_F$) is positive for valence bands and negative for conduction bands. It is clear from the electronic band structure (Fig. 1b, d, g and i) that Co_2VAl and Co_2VGa have parabolic bands in the vicinity of the Fermi level, therefore the carriers exhibit low effective mass and hence high mobility. It has been found that the investigated materials exhibit a maximum carrier concentration in the vicinity of the Fermi level. Usually the temperature difference between two materials is responsible for producing a thermoelectric voltage. To gain high thermoelectric efficiency, it is necessary that the material possesses high electrical conductivity, a large Seebeck coefficient and low thermal conductivity.[46] Therefore, to achieve the highest electrical conductivity, high mobility carriers are required. To achieve this, a material with small effective masses is needed. Therefore, we have calculated the effective mass of electrons (m_e^*) for spin-up and spin-down. Usually we estimated the value of effective mass of electrons from the conduction band minimum curvature. The diagonal elements of the effective mass tensor, m_e^*, for the electrons in the conduction band are calculated following this expression;

$$\frac{1}{m_e^*} = \frac{1\partial^2 E(k)}{\hbar^2 \partial k^2} \quad (1)$$

The effective mass of electrons is assessed by fitting the electronic band structure to a parabolic function eqn (1). The calculated electron effective mass ratio (m_e^*/m_e) around the X point of the BZ is about 0.00846 (0.01075) for the spin-down configuration of Co_2VAl (Co_2VGa), while it is 0.01497 (0.02681) for the spin-up configuration of Co_2VAl (Co_2VGa). Therefore, the spin-up electrons possess higher mobility than those of spin-down. The effective mass ratio of the heavy holes (m_{hh}^*/m_e)-around the Γ point of the BZ is about 0.03036 (0.02873) for Co_2VAl (Co_2VGa). This implies that heavy holes possess lower mobility than the electrons.

concentration while the colored regions correspond to the presence of electrons. The red color represents the highest speed, yellow, green and blue have intermediate speeds whereas the violet color shows the lowest speed; (g) calculated spin-up electronic band structure of the Co_2VGa compound; (h) calculated carrier concentration as a function of chemical potential ($\mu - E_F = \pm 0.2$ eV) at three constant temperatures (300, 600 and 900 K) for the spin-up configuration of the Co_2VGa compound; (i) calculated spin-down electronic band structure of the Co_2VGa compound; (j) calculated carrier concentration as a function of chemical potential ($\mu - E_F = \pm 0.2$ eV) at three constant temperatures (300, 600 and 900 K) for the spin-down configuration of the Co_2VGa compound. We would like to mention that the colors in the electronic band structures mean nothing, they are just to illustrate the bands in a clear way.

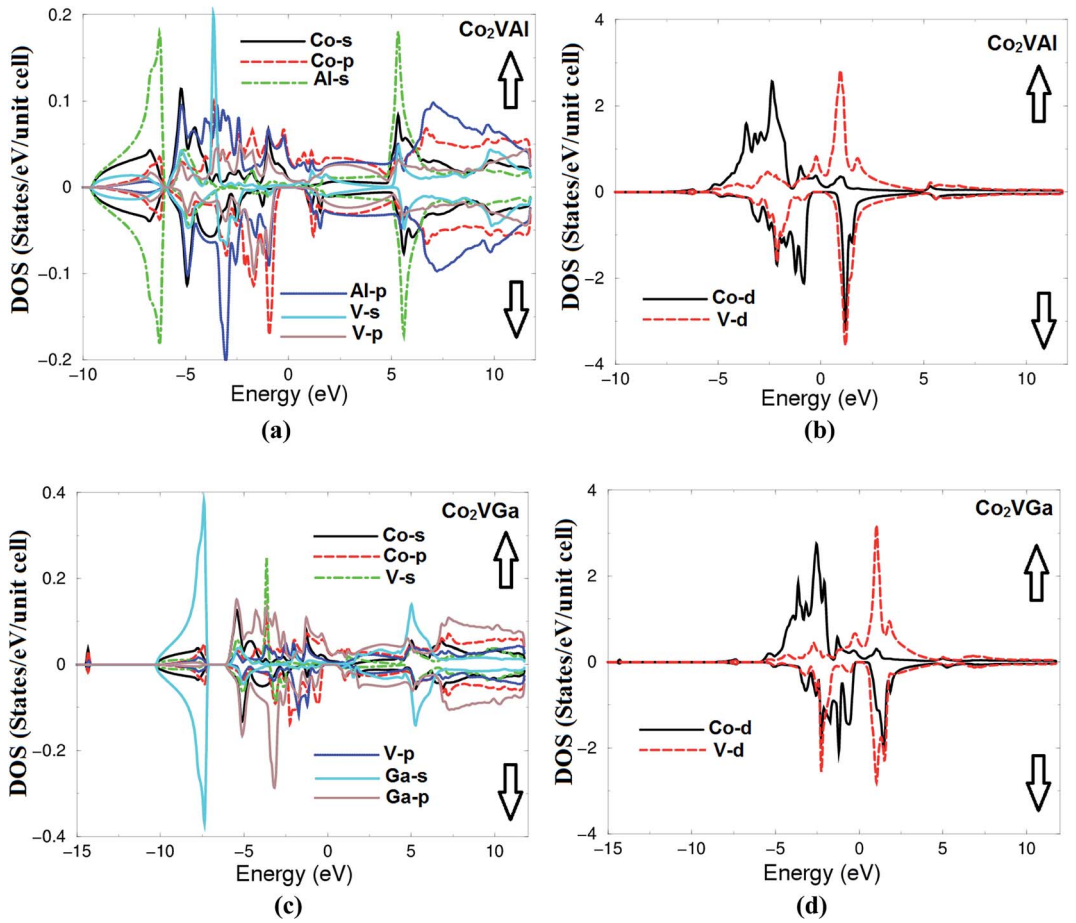

Fig. 2 (a and b) The calculated angular momentum projected density of states (PDOS) of the Co_2VAl compound for the spin up (↑) and spin down (↓) states; (c and d) the calculated angular momentum projected density of states (PDOS) of the Co_2VGa compound for the spin up (↑) and spin down (↓) states.

To ascertain that the investigated Heusler compounds Co_2VAl and Co_2VGa are expected to give maximum efficiency at E_F, we have investigated the electrical conductivity for spin-up/down as a function of temperature at a certain value of chemical potential ($\mu = E_F$) as shown in Fig. 5a–d, which represents the temperature variation of σ/τ. Fig. 5a and b illustrate the electrical conductivity of the two compounds for spin-up. It has been noticed that at low temperature (<100 K) the electrical conductivity of Co_2VAl reduced with increasing temperature, then afterwards a prompt increase occurred with rising temperature. Meanwhile, Co_2VGa shows a sharp rise up to 100 K, then a significant change in the trend of σ/τ occurs to reach the saturated value at around 600 K that is attributed to the different bands which form the Fermi surface as shown in Fig. 1a and f. Meanwhile, for the spin-down configuration (Fig. 5c and d) the compounds have semiconductor like behavior; the electrical conductivity exhibits almost a constant value of about 1.11×10^{15} (3.4×10^{15}) $(\Omega\ ms)^{-1}$ up to 400 (450) K for Co_2VAl (Co_2VGa). Above these temperatures a rapid increase occurs to reach the maximum value of about 4.14×10^{17} (1.30×10^{18}) $(\Omega\ ms)^{-1}$ for Co_2VAl (Co_2VGa) at 900 K. At room temperature the value of σ/τ for spin-down electrons is very low in comparison to the spin-up electrons. Furthermore, we have calculated the total σ/τ. The total σ/τ is computed by using the two current model.[47,48] It is clear that σ/τ (↑) for Co_2VAl (Fig. 5a) shows a slight deviation from the linear temperature dependence, whereas total σ/τ (Fig. 5e) varies almost linearly with temperature. Therefore, at a certain value of chemical potential the carrier concentration and electrical conductivity are temperature-dependent.

In addition to that, we have calculated σ/τ of Co_2VAl and Co_2VGa for spin-up/down electrons as a function of chemical potential ($\mu - E_F = \pm 0.15$ eV) at three constant temperatures (300, 600 and 900 K) as shown in Fig. 5g–j. It is clear that above E_F a significant increase in the electrical conductivity occurs to reach a maximum value of about 1.0×10^{21} (0.92×10^{21}) $(\Omega\ ms)^{-1}$ at $\mu - E_F = +0.15$ eV for spin-up electrons of Co_2VAl (Co_2VGa). Meanwhile, for spin-down electrons it is about 8.5×10^{20} (7.5×10^{20}) $(\Omega\ ms)^{-1}$ for Co_2VAl (Co_2VGa) at $\mu - E_F = +0.15$ eV. It is clear that the temperature has an insignificant influence on the electrical conductivity in the chemical potential ($\mu - E_F$) range between −0.15 eV and +0.15 eV.

3.3.2. Electronic thermal conductivity. The thermal conductivity (k) consists of the electronic contribution k_e (electrons and holes transporting heat) and the phonon contribution k_l (phonons traveling through the lattice). The BoltzTraP code

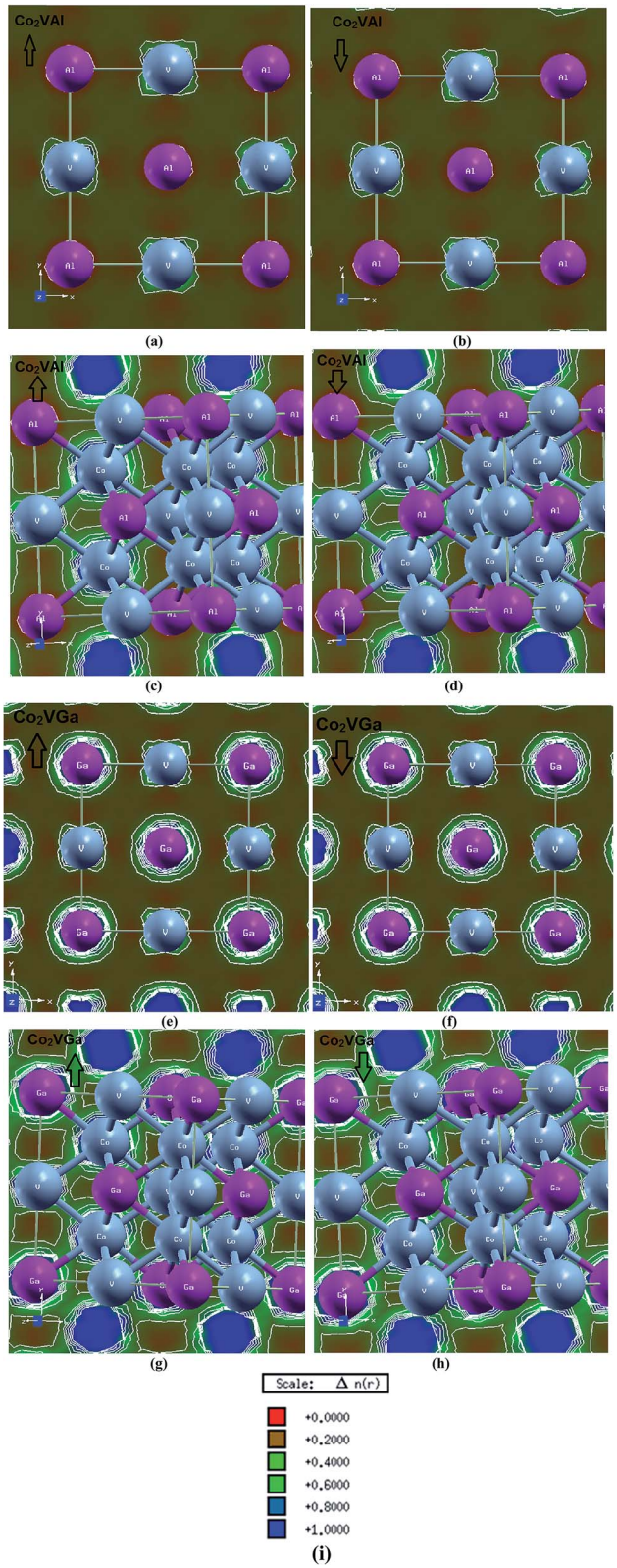

Fig. 3 The calculated valence electronic charge density in two crystallographic planes for spin-up/down configurations: (a and b) the calculated valence electronic charge density for the Co_2VAl compound in the (1 0 0) crystallographic plane for spin-up and spin-down; (c and d) the calculated valence electronic charge density for the Co_2VAl compound in the (1 0 1) crystallographic plane for spin-up and spin-down; (e and f) the calculated valence electronic charge density for the Co_2VGa compound in the (1 0 0) crystallographic plane for spin-up and spin-down; (g and h) the calculated valence electronic charge density for the Co_2VGa compound in the (1 0 1) crystallographic plane for spin-up and spin-down; (i) the thermoscale which shows the value of charge accumulation around the atoms, where the red color exhibits zero charge accumulation (0.0000) while the blue color indicates the maximum charge accumulation (+1.0000), the colors between red and blue represent the degree of charge accumulation between 0.0 and 1.0.

calculates only the electronic part k_e.[31] Using the BoltzTraP code we have calculated the electronic thermal conductivity of Co_2VAl and Co_2VGa for (↑) and (↓) as a function of temperature at the Fermi level (a certain value of chemical potential ($\mu = E_F$)) as shown in Fig. 6a–d which represents the variation in k_e/τ at different temperatures. It is clear that for the spin-up configuration of Co_2VAl and Co_2VGa, k_e/τ increases linearly with increasing temperature. This tendency is not valid for the spin-down configuration (Fig. 6c and d) since k_e/τ exhibits a zero value up to 400 K for Co_2VAl and 450 K for Co_2VGa, then a rapid increase occurs with rising temperature. The results show that the electronic thermal conductivity is temperature-dependent.

In addition to that, we have calculated k_e/τ of Co_2VAl and Co_2VGa for spin-up/down electrons as a function of chemical potential ($\mu - E_F = \pm 0.15$ eV) at three constant temperatures (300, 600 and 900 K) as shown in Fig. 6e–h. It is clear that a significant increase in k_e/τ occurs with increasing temperature and the temperature 900 K induced the highest k_e/τ values, while 300 K induced the lowest k_e/τ values, confirming that 300 K is the optimal temperature which gives the lowest k_e/τ values in the chemical potential range $\mu - E_F = +0.15$ eV.

3.3.3. Seebeck coefficient. The Seebeck coefficient (S) is an important quantity which is related to the electronic band structure of the materials. We have calculated the Seebeck coefficients of Co_2VAl and Co_2VGa as a function of chemical potential ($\mu - E_F = \pm 0.15$ eV) at three constant temperatures (300, 600 and 900 K). In Fig. 7a–d we illustrate S along the chemical potential between 0.15 and −0.15 eV. One can see in the vicinity of E_F that the Seebeck coefficient for the spin-up configuration exhibits several pronounced structures at E_F, below and above E_F. The differences in the structures' height and location between the two compounds is attributed to the Fermi surface's configuration. It has been found that for the spin-up case the Seebeck coefficient of Co_2VGa at around $\mu - E_F = +0.07$ eV exhibits a higher value than that of Co_2VAl. Fig. 7c and d illustrate the Seebeck coefficients of both compounds for the spin-down case. One can see in the vicinity of E_F the Seebeck coefficients exhibit two pronounced structures just below and above E_F, with the highest values of Seebeck coefficient at 300 K (1100.0 and −1000.0 μV K^{-1} for Co_2VAl, and 1000.0 and −800.0 μV K^{-1} for Co_2VGa). It has been noticed that in the Co_2VAl compound a large value (1100 μV K^{-1}) of Seebeck coefficient is obtained for spin-down electrons due to the existence of an almost flat conduction band along the L to Γ direction (see Fig. 1d). It has been found that for both compounds the obtained value of S for spin-down electrons is greater than that of spin-up electrons and the total S of Co_2VAl is larger than that of Co_2VGa. This is attributed to the fact that there are more

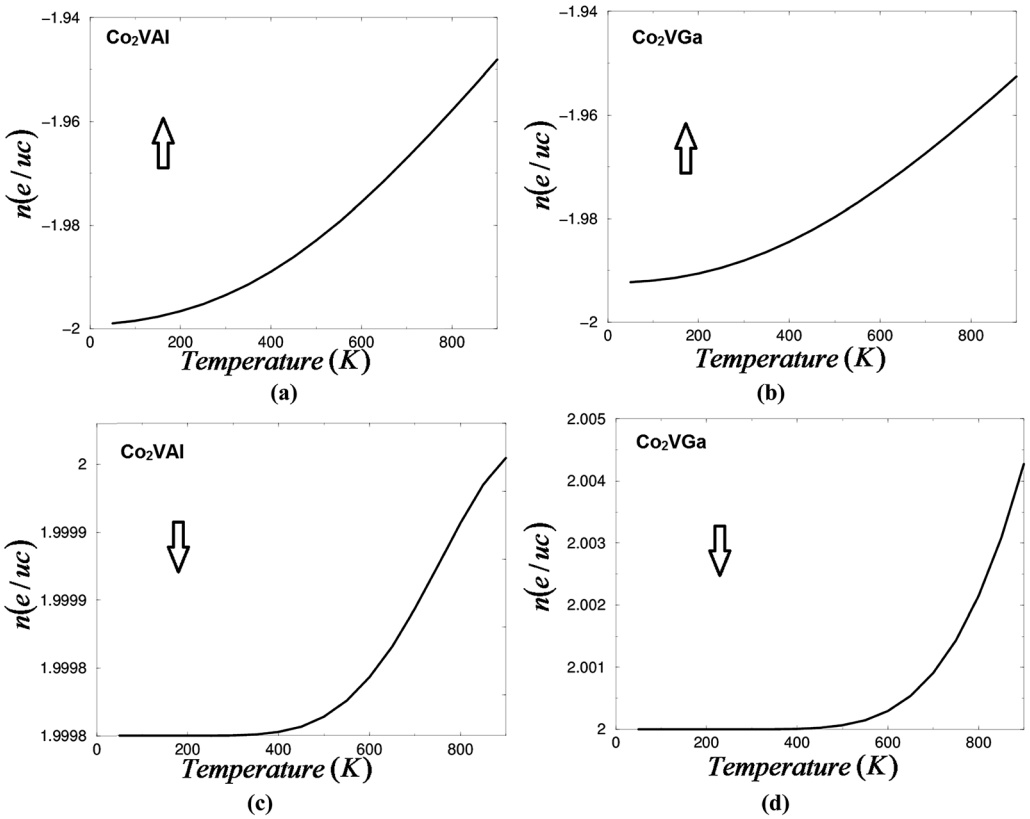

Fig. 4 (a and b) The temperature induced carrier concentration per unit cell (*e* per uc) for spin-up electrons *versus* temperature for the Co_2VAl and Co_2VGa compounds; (c and d) the temperature induced carrier concentration per unit cell (*e* per uc) for spin-down electrons *versus* temperature for the Co_2VAl and Co_2VGa compounds.

valence electrons in Co_2VGa than in Co_2VAl. For an increase in the valence electrons the absolute value of the Seebeck coefficient decreases. This is explained by the increase in the electron concentration in the bands. By increasing the number of valence electrons, additional electrons are added to the d-band at the Fermi energy.[49] This leads to an increase in the carrier concentration. The increase in the carrier concentration leads to a decrease in the Seebeck coefficient.[46] The interrelationship between carrier concentration and Seebeck coefficient can be seen from relatively simple models of electron transport. For simple metals or degenerate semiconductors with parabolic bands and energy independent scattering, the Seebeck coefficient S is given by;

$$S = \frac{8\pi^2 {k_B}^2}{3eh^2} m^* T \left(\frac{\pi}{3n}\right)^{3/2} \quad (2)$$

where n is the carrier concentration and m^* is the effective mass of the carrier. It can be clearly seen that S depends on the carrier concentration and on the effective mass m^*. The latter depends on the shape of the bands.

From Fig. 7a–d it is clear that the obtained values of Seebeck coefficients are negative/positive for the entire range of the chemical potential suggesting the presence of n/p-type charge carriers. For spin-up electrons the temperature has a significant influence on S along the chemical potential range $\mu - E_F = \pm 0.15$ eV, whereas for the spin-down electrons the temperature shows a significant influence in the chemical potential range between +0.05 eV and −0.05 eV only.

From the above, we should emphasize that both materials posses n-/p-type conductions in the vicinity of E_F. The sign of S indicates the type of dominant charge carriers: S with a positive sign represents the p-type materials, whereas n-type materials have a negative S.[21,31,50,51]

3.3.4. Power factor. The power factor is defined as $P = S^2\sigma/\tau$, where S^2 is the Seebeck coefficient's square, σ is the electrical conductivity and τ is the relaxation time. Following this formula one can see that P is directly proportional to S^2 and σ/τ. Therefore, in order to gain a high power factor one needs to maintain the values of S^2 and σ/τ. It is well known that the figure of merit is a very important quantity for calculating the transport properties of materials. The dimensionless figure of merit is written as $ZT = S^2\sigma T/k_e + k_l$ (ref. 40 and 52), which shows that the power factor comes in the numerator of the figure of merit, thus the power factor is an important quantity and plays a principle role in evaluating the transport properties of the materials.

In order to ascertain the influence of varying the chemical potential on the power factor, we have calculated the power factor for spin-up and spin-down at three fixed temperatures (300, 600 and 900 K) as a function of chemical potential ($\mu - E_F$) between −0.15 and +0.15 eV as shown in Fig. 8a–d. It has been found that the investigated material exhibits the highest power factor just above and below E_F. It is interesting to see that

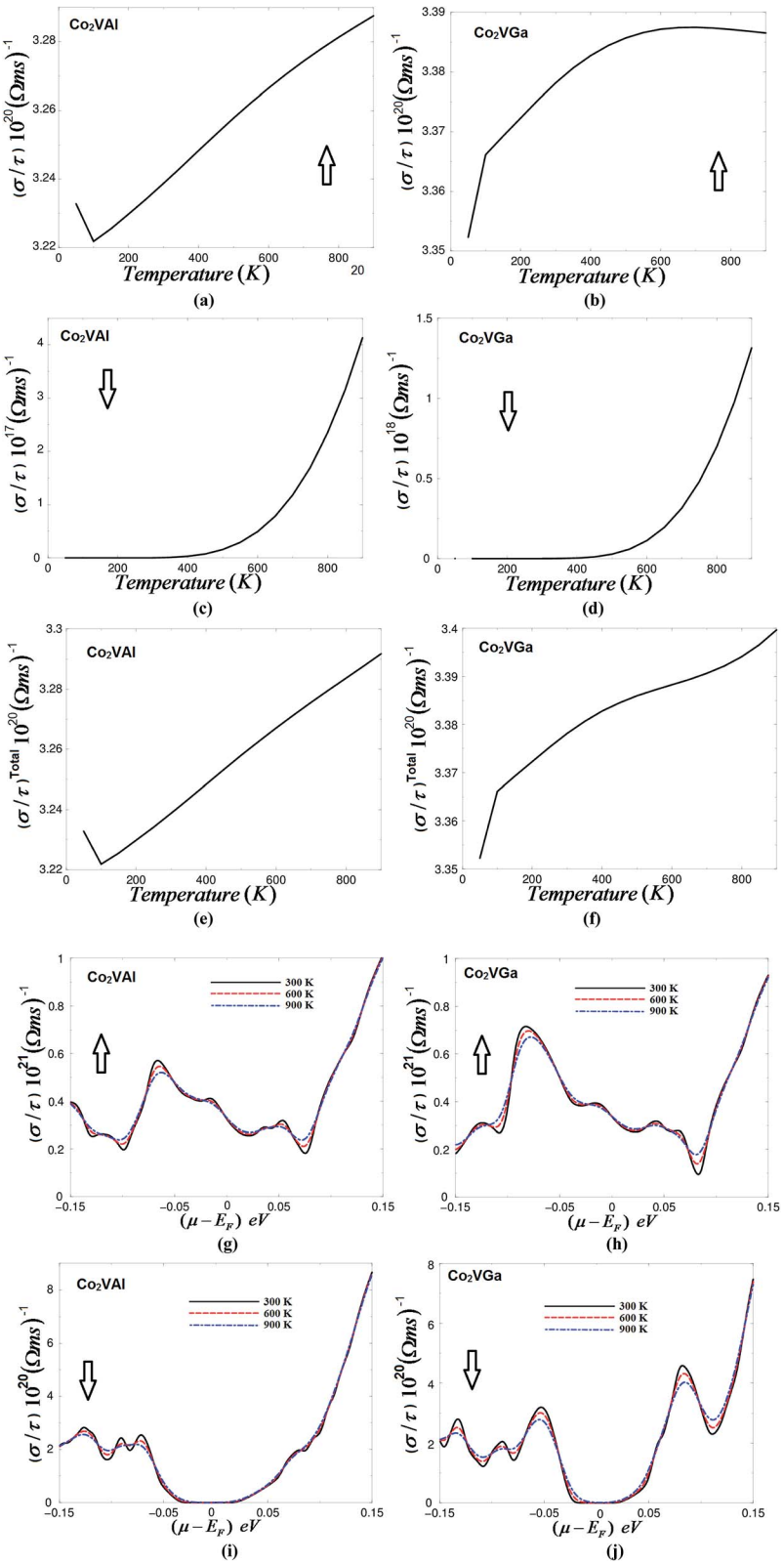

Fig. 5 (a and b) The electrical conductivity for spin-up electrons *versus* temperature for the Co_2VAl and Co_2VGa compounds; (c and d) the electrical conductivity for spin-down electrons *versus* temperature for the Co_2VAl and Co_2VGa compounds; (e and f) the total electrical conductivity *versus* temperature for the Co_2VAl and Co_2VGa compounds; (g and h) the electrical conductivity of Co_2VAl and Co_2VGa for spin-up electrons as a function of chemical potential ($\mu - E_F = \pm 0.15$ eV) at three constant temperatures (300, 600 and 900 K); (i and j) the electrical conductivity of Co_2VAl and Co_2VGa for spin-down electrons as a function of chemical potential ($\mu - E_F = \pm 0.15$ eV) at three constant temperatures (300, 600 and 900 K).

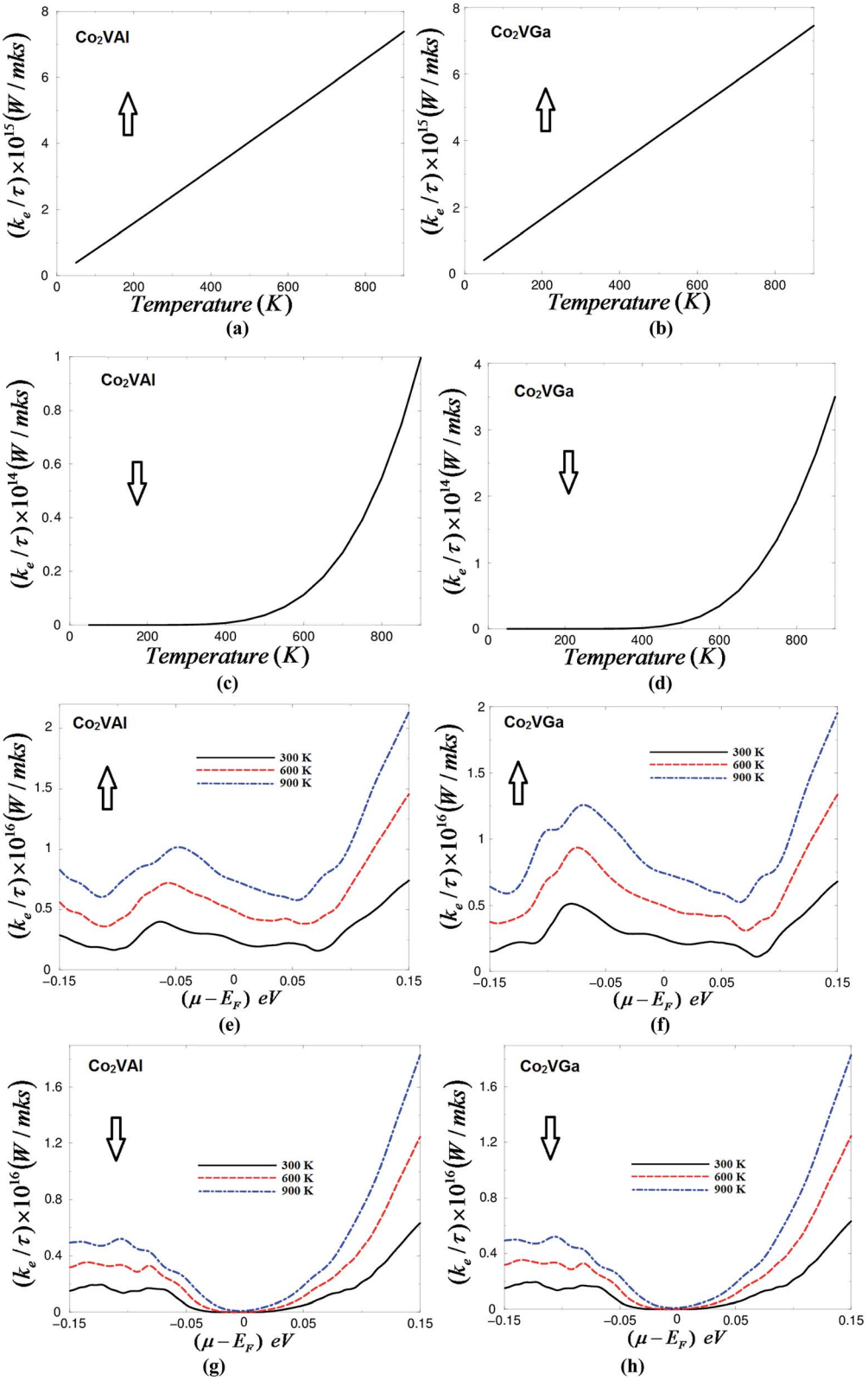

Fig. 6 (a and b) The electronic thermal conductivity for spin-up electrons *versus* temperature for the Co_2VAl and Co_2VGa compounds; (c and d) the electronic thermal conductivity for spin-down electrons *versus* temperature for the Co_2VAl and Co_2VGa compounds; (e and f) the electronic thermal conductivity of Co_2VAl and Co_2VGa for spin-up electrons as a function of chemical potential ($\mu - E_F = \pm 0.15$ eV) at three constant temperatures (300, 600 and 900 K); (g and h) the electronic thermal conductivity of Co_2VAl and Co_2VGa for spin-down electrons as a function of chemical potential ($\mu - E_F = \pm 0.15$ eV) at three constant temperatures (300, 600 and 900 K).

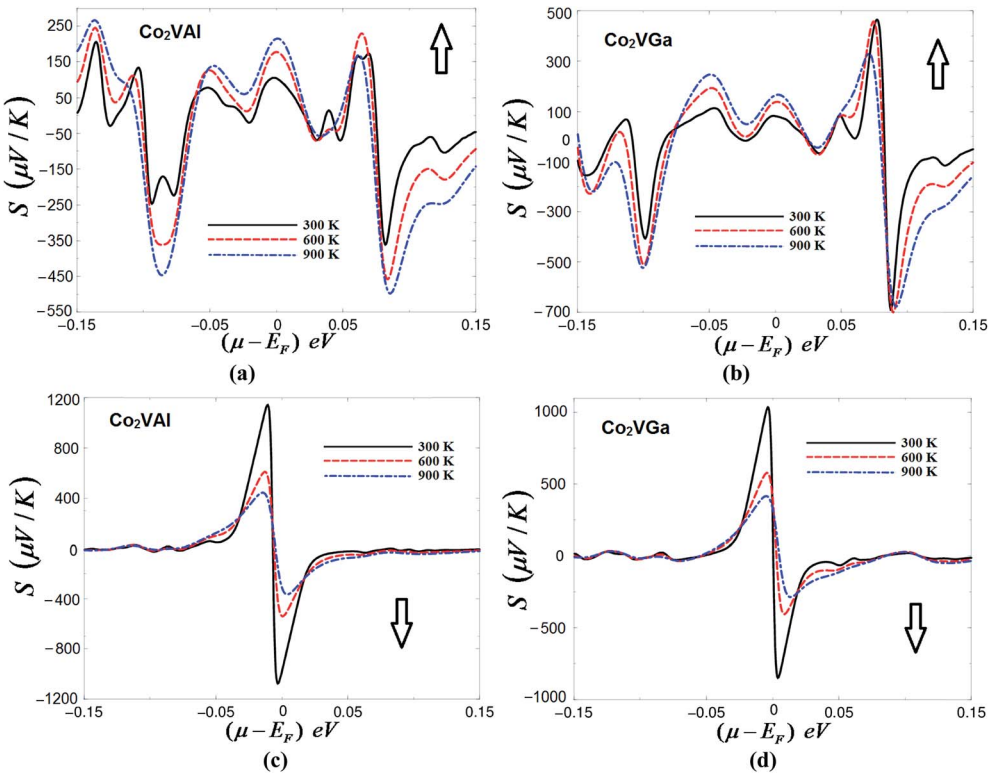

Fig. 7 (a and b) The Seebeck coefficient of Co_2VAl and Co_2VGa for spin-up electrons as a function of chemical potential ($\mu - E_F = \pm 0.15$ eV) at three constant temperatures (300, 600 and 900 K); (c and d) the Seebeck coefficient of Co_2VAl and Co_2VGa for spin-down electrons as a function of chemical potential ($\mu - E_F = \pm 0.15$ eV) at three constant temperatures (300, 600 and 900 K).

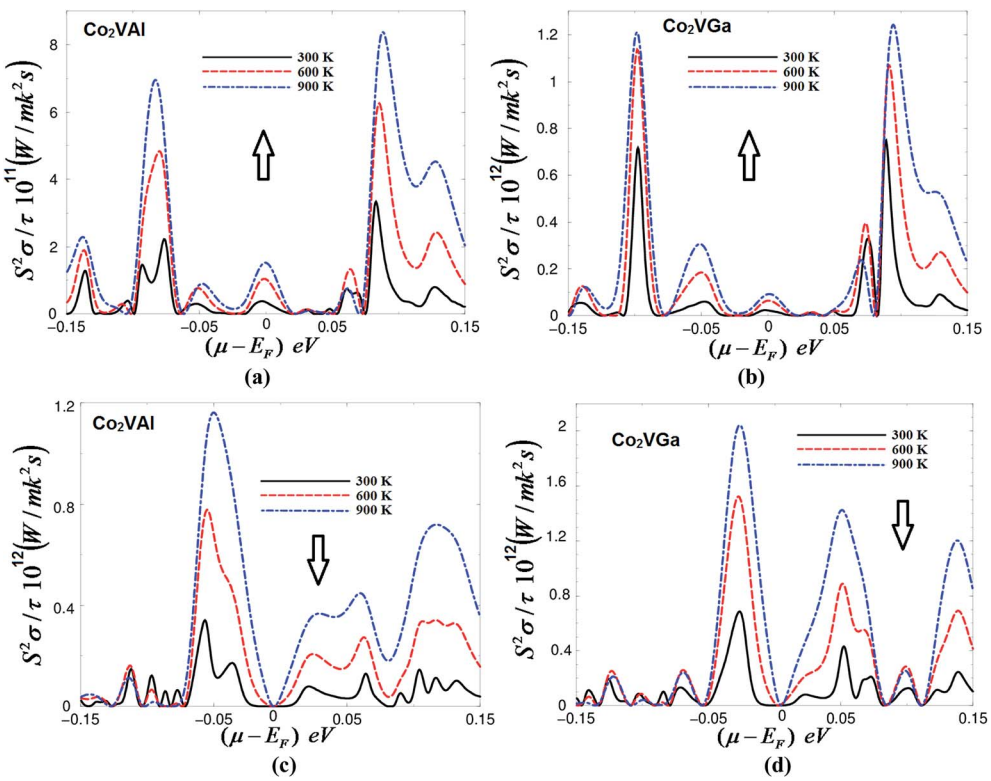

Fig. 8 (a and b) The power factor of Co_2VAl and Co_2VGa for spin-up electrons as a function of chemical potential ($\mu - E_F = \pm 0.15$ eV) at three constant temperatures (300, 600 and 900 K); (c and d) the power factor of Co_2VAl and Co_2VGa for spin-down electrons as a function of chemical potential ($\mu - E_F = \pm 0.15$ eV) at three constant temperatures (300, 600 and 900 K).

increasing the temperature causes significant increases in the power factor. The increase in the Seebeck coefficient also leads to a maximum of the power factor at $\mu - E_F = \pm 0.05$ eV for Co_2VAl (Fig. 8c) and at -0.03 eV and 0.05 eV for Co_2VGa (Fig. 8d). It is slightly shifted compared to the maximum of the Seebeck coefficient due to the decreased conductivity.

We would like to mention here that in our previous works[53–56] we have calculated the transport properties using the FPLAPW method within the BoltzTraP code on several systems whose transport properties are known experimentally, and in those previous calculations we found very good agreement with the experimental data. Thus, we believe that our calculations reported in this paper would produce very accurate and reliable results.

4. Conclusions

We have calculated the spin-polarized electronic band structure of Co_2VAl and Co_2VGa and hence the transport properties based on the semi-classical Boltzmann theory as incorporated within the BoltzTraP code. The calculated spin-polarized electronic band structure reveals that these compounds possess parabolic bands in the vicinity of the Fermi level, therefore the carriers exhibit low effective mass and hence high mobility. It has been found that the transport coefficients increase/reduce with increasing temperature, therefore the spin-up/down transport coefficients are temperature-dependent. The minority spin density of states at E_F, $N(E_F)$ vanishes for Co_2VAl and Co_2VGa which should lead to unusual transport properties because only the majority density contributes to the states at E_F. The calculated valence band's electronic charge density distribution reveals that there exists a strong covalent bond between the atoms which is more favorable for the transport of carriers than an ionic one. Calculations show that Co_2VAl exhibits a higher Seebeck coefficient than that obtained from Co_2VGa. The increase in the Seebeck coefficient also leads to a maximum power factor. This makes them attractive candidates for materials used in spin voltage generators.

Acknowledgements

The result was developed within the CENTEM project, reg. no. CZ.1.05/2.1.00/03.0088, co-funded by the ERDF as part of the Ministry of Education, Youth and Sports OP RDI programme and, in the follow-up sustainability stage, supported through CENTEM PLUS (LO1402) by financial means from the Ministry of Education, Youth and Sports under the National Sustainability Programme I. Computational resources were provided by MetaCentrum (LM2010005) and CERIT-SC (CZ.1.05/3.2.00/08.0144) infrastructures.

References

1 M. I. Katsnelson, V. Y. Irkhin, L. Chioncel and R. A. de Groot, *Rev. Mod. Phys.*, 2008, **80**, 315.
2 C. Felser, G. H. Fecher and B. Balke, *Angew. Chem., Int. Ed.*, 2007, **46**, 668.
3 B. Balke, S. Wurmehl, G. H. Fecher, C. Felser and J. Kübler, *Sci. Technol. Adv. Mater.*, 2008, **9**, 014102.
4 Y. Miura, K. Nagao and M. Shirai, *Phys. Rev. B: Condens. Matter Mater. Phys.*, 2004, **69**, 144413.
5 H. C. Kandpal, V. Ksenofontov, M. Wojcik, R. Seshadri and C. Felser, *J. Phys. D: Appl. Phys.*, 2007, **40**, 1587.
6 S. Picozzi, A. Continenza and A. J. Freeman, *Phys. Rev. B: Condens. Matter Mater. Phys.*, 2004, **69**, 094423.
7 P. J. Webster, *Contemp. Phys.*, 1969, **10**, 559.
8 G. E. Bacon and J. S. Plant, *J. Phys. F: Met. Phys.*, 1971, **1**, 524.
9 P. J. Webster and K. R. A. Ziebeck, *Landolt-Börnstein new series group III*, 1988, vol. 19c, p. 75.
10 K. R. A. Ziebeck and K. U. Neumann, *Landolt-Börnstein new series group III*, 2001, vol. 32c, p. 64.
11 T. Graf, F. Casper, J. Winterlik, B. Balke, G. H. Fecher and C. Felser, *Z. Anorg. Allg. Chem.*, 2009, **635**, 976.
12 A. Sozinov, A. A. Likhachev, N. Lanska and K. Ullako, *Appl. Phys. Lett.*, 2002, **80**, 1746.
13 A. Planes and J. Ortin, *J. Appl. Phys.*, 1992, **71**, 950.
14 R. Kainuma, H. Nakano, K. Oikawa, K. Ishida and T. Nishizawa, *Mater. Res. Soc. Symp. Proc.*, 1992, **246**, 403.
15 R. Kainuma, N. Ono and K. Ishida, *Mater. Res. Soc. Symp. Proc.*, 1995, **360**, 467.
16 R. Kainuma, H. Nakano and K. Ishida, *Metall. Mater. Trans. A*, 1996, **27**, 4153.
17 K. Uchida, S. Takahashi, K. Harii, J. Ieda, W. Koshibae, S. Ando, K. Maekawa and E. Saitoh, *Nature*, 2008, **455**, 778.
18 S. A. Wolf, D. D. Awschalom, R. A. Buhrman, J. M. Daughton, S. von Molnar, M. L. Roukes, A. Y. Chtchelkanova and D. M. Treger, *Science*, 2001, **294**, 1488.
19 I. Zutic, J. Fabian and S. D. Sarma, *Rev. Mod. Phys.*, 2004, **76**, 323.
20 C. Chappert, A. Fert and F. N. Van Dau, *Nat. Mater.*, 2007, **6**, 813.
21 S. Sharma and S. K. Pandey, *J. Phys.: Condens. Matter*, 2014, **26**, 215501.
22 P. J. Webster and K. R. A. Ziebeck, *J. Phys. Chem. Solids*, 1973, **34**, 1647.
23 P. J. Webster and K. R. A. Ziebeck, *Alloys and compounds of d elements with Main Group Elements, Part 2*, ed. H. R. J. Wijn and Landolt-Bornstein, Springer Berlin, New Series, Group III, 1998, 2001, vol. 19/c, pp. 75–184.
24 J. P. Perdew, S. Burke and M. Ernzerhof, *Phys. Rev. Lett.*, 1996, **77**, 3865.
25 P. Blaha, K. Schwarz, G. K. H. Madsen, D. Kvasnicka and J. Luitz, WIEN2k, *An augmented plane wave plus local orbitals program for calculating crystal properties*, Vienna University of Technology, Austria, 2001.
26 V. I. Anisimov, I. V. Solvyev, M. A. Korotin, M. T. Czyzyk and C. A. Sawatzky, *Phys. Rev. B: Condens. Matter Mater. Phys.*, 1993, **48**, 16929.
27 A. I. Liechtenstein, V. I. Anisimov and J. Zaanen, *Phys. Rev. B: Condens. Matter Mater. Phys.*, 1995, **52**, R5467.
28 O. K. Andersen, *Phys. Rev. B: Condens. Matter Mater. Phys.*, 1975, **12**, 3060.
29 J. P. Perdew and Y. Wang, *Phys. Rev. B: Condens. Matter Mater. Phys.*, 1992, **45**, 13244.

30 D. P. Rai, Sandeep, A. Shankar, M. P. Ghimire and R. K. Thapa, *Phys. Scr.*, 2012, **86**, 045702.
31 G. K. H. Madsen and D. J. Singh, *Comput. Phys. Commun.*, 2006, **175**, 67–71.
32 P. B. Allen, in *Quantum Theory of Real Materials*, ed. J. R. Chelikowsky and S. G. Louie, Kluwer, Boston, 1996, pp. 219–250.
33 J. M. Ziman, *Electrons and Phonons*, Clarendon, Oxford, 2001.
34 C. M. Hurd, *The Hall Effect in Metals and Alloys*, Plenum, New York, 1972.
35 K. J. Plucinski, I. V. Kityk, J. Kasperczyk and B. Sahraoui, *Semicond. Sci. Technol.*, 2001, **16**, 467.
36 H. S. Saini, M. Singh, A. H. Reshak and M. K. Kashyap, *J. Magn. Magn. Mater.*, 2013, **331**, 1–6.
37 Y. Saeed, S. Nazir, A. Shaukat and A. H. Reshak, *J. Magn. Magn. Mater.*, 2010, **322**, 3214–3222.
38 C. Felser and G. H. Fecher, *Spintronics From Materials to Devices*, Springer Dordrecht Heidelberg, New York London, eBook, 2013, DOI: 10.1007/978-90-481-3832-6, ISBN 978-90-481-3831-9, ISBN 978-90-481-3832-6.
39 J. Kübler, A. R. Williams and C. B. Sommers, *Phys. Rev. B: Condens. Matter Mater. Phys.*, 1983, **28**, 1745.
40 A. H. Reshak and S. Azam, *J. Magn. Magn. Mater.*, 2013, **342**, 80–86.
41 J.-H. Lee, G. Wu and J. C. Grossman, *Phys. Rev. Lett.*, 2010, **104**, 016602.
42 A. H. Reshak, Z. A. Alahmed, J. Bila, V. V. Atuchin, B. G. Bazarov, O. D. Chimitova, M. S. Molokeev, I. P. Prosvirin and A. P. Yelisseyev, *J. Phys. Chem. C*, 2016, **120**, 10559–10568.
43 Schlusseltechnologien Key Technologies, *41st IFF Springschool*, 2010, pp. A1–18.
44 S. Khan and A. H. Reshak, *Polyhedron*, 2015, **85**, 962–970.
45 F. Wu, H. Z. Song, J. F. Jia and X. Hu, *Prog. Nat. Sci.*, 2013, **23**(4), 408–412.
46 G. J. Snyder and E. S. Toberer, *Nat. Mater.*, 2008, **7**, 105–114.
47 H. J. Xiang and D. J. Singh, *Phys. Rev. B: Condens. Matter Mater. Phys.*, 2007, **76**, 195111.
48 A. S. Botana, P. M. Botta, C. D. L. Calle, A. Pineiro, V. Pardo, D. Baldomir and J. A. Alonso, *Phys. Rev. B: Condens. Matter Mater. Phys.*, 2011, **83**, 184420.
49 S. Ouardi, B. Balke, A. Gloskovskii, G. H. Fecher, C. Felser, G. Schönhense, T. Ishikawa, T. Uemura, M. Yamamoto, H. Sukegawa, W. Wang, K. Inomata, Y. Yamashita, H. Yoshikawa, S. Ueda and K. Kobayashi, *J. Phys. D: Appl. Phys.*, 2009, **42**, 084010.
50 B. Xu, X. Li, G. Yu, J. Zhang, S. Ma, Y. Wang and L. Yi, *J. Alloys Compd.*, 2013, **565**, 22–28.
51 T. J. Scheidemantel, C. Ambrosch-Draxl, T. Thonhauser, J. V. Badding and J. O. Sofo, *Phys. Rev. B: Condens. Matter Mater. Phys.*, 2003, **68**, 125210.
52 C. Calvin Hu, *Modern Semiconductor Devices for Integrated Circuits, Part I: Electrons and holes in a semiconductor*, November 11, 2011.
53 A. H. Reshak and S. Auluck, *Comput. Mater. Sci.*, 2015, **96**, 90–95.
54 A. H. Reshak, *J. Phys. Chem. Solids*, 2015, **78**, 46–52.
55 A. H. Reshak, *Renewable Energy*, 2015, **76**, 36–44.
56 A. H. Reshak, *RSC Adv.*, 2014, **4**, 63137; A. H. Reshak, *RSC Adv.*, 2015, **5**, 47569.